Enhancing Photoacoustic Visualisation of Clinical Needles with Deep Learning

Mengjie Shi*¶, Zhaoyang Wang†, Tianrui Zhao*, Simeon J. West‡, Adrien E. Desjardins§, Tom Vercauteren* and Wenfeng Xia*
*School of Biomedical Engineering and Imaging Sciences, King's College London, London, UK
†Department of Computer Science, Whiting School of Engineering, Johns Hopkins University, Baltimore, US
‡Department of Anaesthesia, University College Hospital, London, UK
§Department of Medical Physics and Biomedical Engineering, University College London, London, UK
¶Email: mengjie.shi@kcl.ac.uk

***Abstract*—Photoacoustic imaging has shown great potential in guiding various minimally invasive procedures by providing complementary information to ultrasound imaging, visualising critical tissue targets as well as surgical tools such as metallic needles with rich optical contrast. The use of light emitting diodes (LEDs) as excitation sources further accelerates the clinical translation of this modality due to its favorable affordability, portability, and cost-efficiency but results in the degradation of image quality associated with low pulse energy. In this work, we propose a framework based on a modified U-Net to enhance the visualisation of clinical metallic needles with a commercial LED-based photoacoustic and ultrasound imaging system. This framework included the generation of semi-synthetic datasets combining both simulated data and *in vivo* measurements. Evaluation of the trained neural network was performed with needle insertions into a blood-vessel-mimicking phantom, and pork joint *ex vivo* tissue. This deep learning-based framework significantly enhanced the visualisation of the needle with photoacoustic imaging, achieving 4.3- and 3.2-times higher signal-to-noise ratios (SNRs) compared to conventional reconstructions, which could be helpful for guiding minimally invasive procedures.**

***Index Terms*—Photoacoustic imaging, needle visualisation, deep learning, light emitting diode, minimally invasive procedures**

I. Introduction

Ultrasound (US) imaging is widely used for guiding minimally invasive percutaneous surgeries such as peripheral nerve blocks [1], interventional biopsy [2] and diagnostic prenatal test [3]. During these surgeries, a clinical needle is inserted into the human body under real-time US guidance. However, clinical challenges with US imaging here include the poor visibility of critical tissue structures such as nerves and small blood vessels due to the insufficient contrast from their surroundings, and invasive surgical devices such as clinical needles. For example, clinical needles with steep insertion angles can cause US reflections away from the transducer aperture, leading to poor ultrasound visibility. Loss of visualisation of the tissue targets or the invasive surgical devices can result in significant complications [4].

Photoacoustic (PA) imaging has been of growing interest in recent decades for its potential preclinical and clinical applications [5]. In recent years, several research groups have proposed the combination of US and PA imaging for guiding minimally invasive procedures by offering complementary information to each other, with US imaging proving tissue structural information and PA imaging highlighting critical tissue structures and invasive surgical devices such as metallic needles [6, 7]. Recently, laser diodes and light-emitting diodes (LEDs) have shown promise to facilitate the clinical transition with their compact size, effective cost and less irradiation [8, 9]. However, compared to the conventional laser excitation sources, LEDs have much lower pulse energy, resulting in lower signal-to-noise (SNR) ratio.

Recently, deep learning (DL) has been used by several groups to improve the image quality of PA imaging systems [10–14]. Dataset plays an important role when applying DL-based methods for image enhancement in PA imaging. Simulated data are commonly used in the context of deep learning, as they can be generated in large quantity with lots of variations. Most importantly, manual annotation with gold standard expertise is needless. Various types of simulation tools have been developed and applied to obtain simulated data for training [15–17]. However, the degree of realism is limited by simulation approaches and it is still challenging to translate the models trained on pure simulated data to various *in vivo* scenarios.

In this paper, we proposed a DL-based framework to enhance the visualisation of clinical needles with PAI for *in vivo* applications. We developed a hybrid method for generating semi-synthetic datasets and validated its performance with tissue-mimicking phantoms and *ex vivo* tissue. To the best of our knowledge, this is the first work that explores DL for improving needle visualisation with PAI and utilises semi-synthetic datasets for the proposed DL-based framework.

II. Materials and Methods

The generation of semi-synthetic data can be divided into two parts. One part contains the process of acquiring synthetic sensor data for the needles while the other part includes *in vivo* data collection for the background tissue. For simulating the sensor data of the needles, images of simulated needle were first created with different insertion depths and angles. Here, the depths were spanned from 5 mm to 25 mm with

978-0-7381-1209-1/21/$31.00 ©2021 IEEE

an increment of 5 mm; and for each depth, the angles varied from 20 degrees to 65 degrees with steps of 5 degrees.

The optical fluence distributions on the needle shaft were generated using the MCML—Monte Carlo modeling of steady-state light transport in multi-layered tissues [15]. A 4.0×4.0 cm single-layer area was constructed with background optical properties selected from the standard tissue at the wavelength of 850 nm. The refractive index, scattering coefficient and anisotropy were set to 1.4, 100 cm^{-1} and 0.9 according to Ref. [18]. Three absorption coefficients of 0.1, 0.15, 0.2 were selected by adjusting the volume fractions of water and blood. A homogeneous photon beam with a finite size was applied to the surface of the simulation area. Each simulation was run for around 10 minutes with approximate 100 000 photon packets traced per time.

Finally, the optical fluence distributions were taken and multiplied with the simulated needles as the corresponding images of initial pressure distribution, which was later used for forward simulation in the k-Wave toolbox [17]. The photoacoustic waves were generated and propagated through a homogenous medium and received by a 2D linear array-based transducer which was specified with 128 elements (with a pitch of 0.3 mm for each element over 38.4 mm) and a central frequency of 9 MHz with a bandwidth of 80.9% based on the specifications of an LED-based PA/US imaging system AcousticX (see Sec. II. B). The RF data collected by the transducer elements were successively downsampled to 40 MHz, the same as the sampling rate of data acquisition module in AcousticX.

In vivo data were collected by imaging the fingers of 13 healthy human volunteers using AcousticX. Finally, the RF data from the simulated needles and human fingers were added and applied for offline image reconstruction in Fourier domain [19].

Following the workflow, a total number of 2000 semi-synthetic images with substantial variations on both the needle targets and background were prepared. The dataset for training and testing is given by 2000 image pairs that formed by these semi-synthetic images and their corresponding needle images with initial pressure distributions.

A. Network architecture and implementation

The deep neural network used for this work was modified from an established deep neural network based on U-Net [20]. This network had 3 scales in total. Following an encoder path, each scale consisted of two convolutional layers followed by a 2×2 max pooling layer. For the decoder path, similarly, each scale contained two convolutional layers but followed by a transposed convolutional layer with an up-sampling factor of 2. Our network was firstly trained with the input pairs of 128×128 pixels, then applied on unseen real data with a size of 256×256 pixels for further validations.

Implementation of our network was performed in Python using PyTorch v1.2.0. Training was performed for 5000 iterations with a batch size of 4 that minimised Mean Square Error (MSE) Loss using ADAM optimizer (Initial learning rate: 0.001) and on Google CoLaboratory platform using one Tesla P100-PCIE-16GB GPU.

B. Acquisition of phantom and ex vivo data for validation

Evaluation of the trained neural network was implemented on acquired PA images using AcousticX (CYBERDYNE INC, Tsukuba, Japan) with needle insertions (20 gauge needle, BD, USA) into a specially prepared phantom, and pork joint tissue *ex vivo*. For each experiment, raw PA and US data were save and reconstructed offline for further processing.

A blood-vessel-mimicking phantom were prepared for validating the performance of the trained neural network. This phantom was created by arranging several carbon fibre bundles in a plastic box filled with 1% Intralipid dilution [21], which had an optical reduced scattering coefficient of 0.96 mm^{-1} at 850 nm.

C. Evaluation protocol and metrics

Several metrics were calculated for quantifying the performance of the trained neural network on real data. First, to measure the network's performance on artefacts removal, the SNR of the needle shaft was calculated with PA images acquired by conventional reconstruction and the trained neural network respectively. The SNR was defined as SNR = S/σ, where S is the mean of signal amplitude and σ is the standard deviation of noise amplitude. The signal region was chosen with respect to the ground truth where the needle was annotated as a rectangular area according to its real size. The noise region was chosen as the area excluding the signal region. Second, as measures of the accuracy and precision of the needle's location, quantitative metrics such as True Positive Rate (TPR), Positive Predictive Value (PPV), Intersection over Union (IoU) and Average Surface Distance (ASD) were calculated.

III. Experimental results

A. Blood-vessel-mimicking phantom

Compared to conventional reconstruction, the improvements by U-Net enhancement were quite noticeable in term of removing the background noise and the artefacts around the needle. Additionally, the trained neural network precisely identified and reconstructed the needle without being substantially affected by the background artificial vessels that can also be regarded as line targets in the PA images (Fig. 1). As shown by the overlays, the spatial locations of the needle on U-Net enhancement corresponded well to those on conventionally reconstructed images and provided additional indications on US images where the needle was barely visible.

SNR and a series of metrics that commonly used for image segmentation were calculated and reported in Table. I. The SNR values of U-Net enhancement were significantly higher than those of conventional reconstruction. Other metrics especially PPV which represents the accuracy out of all positive predictions, i.e., the needle, showed a great improvement on U-Net enhancement over conventional reconstruction from 3.1%

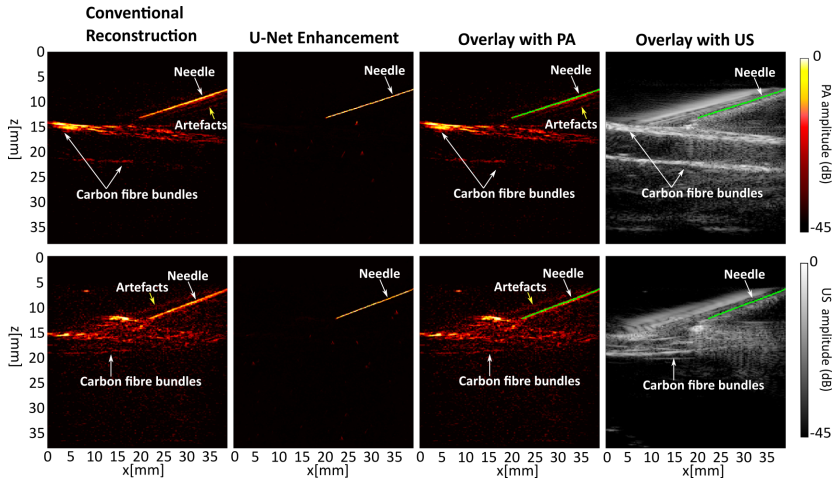

Fig. 1: Photoacoustic imaging with needle insertions into blood-vessel-mimicking phantoms with conventional reconstruction and U-Net enhancement.

TABLE I: Quantitative evaluation of the trained neural network using a blood-vessel-mimicking phantom.

Metrics	Conventional Reconstruction	U-Net Enhancement
SNR	6.289	26.877
IoU	8.5%	31.1%
TPR	89.7%	46.9%
PPV	8.6%	47.8%
ASD	9.060E+05	5015.793

TABLE II: Quantitative evaluation of the trained neural network using *ex* vivo tissue

Metrics	Conventional Reconstruction	U-Net Enhancement
SNR	11.755	37.172
IoU	13.4%	36.6%
TPR	86.0%	45.1%
PPV	14.1%	54.4%
ASD	7.438E+05	2628.722

to 47.8%. It is noted that U-Net enhancement had a worse performance on TPR, compared to conventional reconstruction. Moreover, ASD was calculated and compared across different methods. For conventional reconstruction, the ASD value was exceptionally large due to the background signals. However, this metric decreased with the proposed network.

B. Pork joint tissue ex vivo

Fig.2 and Table.II demonstrates the qualitative and quantitative performances of the trained network using images from *ex vivo* tissue. When inserting into the pork joint, due to the presence of a gap between the imaging probe and the skin surface of the joint, the insertion depth was larger than that with the blood vessel phantom, causing the degradation of the acquired PA images. However, good performance was maintained with the trained U-Net in terms of suppressing the background noise and enhancing the needle visualisation as shown Table.II. Compared to conventionally reconstructed images, images enhanced by the trained model produced a higher SNR value (i.e. 11.755 and 37.172 respectively). The trained neural network also achieved substantial improvements in terms of needle segmentation with the PPV of 54.4% which was 2.8% higher than that of conventional reconstruction.

IV. Discussion and Conclusions

In this work, we developed a deep learning framework to improve the visualisation of clinical metallic needles with photoacoustic imaging. Previous work about applying deep learning methods in this field mainly focused on PA image reconstruction and post-processing such as denoising where simulated data or *ex vivo* data collected from *ex vivo* tissues or phantoms were commonly used for training. Validations were conducted using unseen *ex vivo* or *in vivo* data with simple targets and plain backgrounds, but quantitative analysis was barely included since the acquisition of the corresponding ground truth with gold standard was almost impossible. In this study, differing from prior works, we proposed a hybrid method with a semi-synthetic training dataset. Qualitative and quantitative performance analysis suggested that the neural network trained with this semi-synthetic dataset generalized well on unseen phantom and *ex vivo* data. The proposal model significantly improved the PA image quality by accurately segmenting the needle as well as substantially suppressed the background noise and artefacts.

Visualisation of the needle especially the shaft was greatly enhanced by our proposed framework, but the visibility of the needle tip was still limited to a depth of around 1 cm. In the future, a fibre-optic ultrasound transmitter with a coated distal end could be integrated with the needle for enhancing its tip [22]. Light-absorbing coatings based on elastomeric nanocomposites [23] could also be applied to the needle shaft for enhancing its visibility for guiding minimally invasive procedures.

Acknowledgment

This work was supported by Wellcome Trust [203148/Z/16/Z, WT101957], EPSRC (NS/A000027/1,

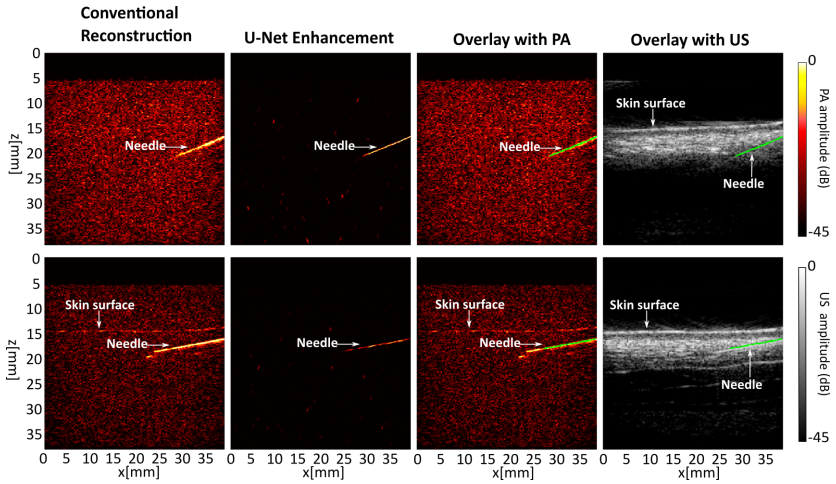

Fig. 2: Photoacoustic imaging with needle insertions into *ex vivo* tissue with conventional reconstruction and U-Net enhancement.

NS/A000049/1) and King's – China Scholarship Council PhD Scholarship program (K-CSC).

REFERENCES

[1] K. J. Chin, A. Perlas, V. W. S. Chan, and R. Brull, "Needle Visualization in Ultrasound-Guided Regional Anesthesia: Challenges and Solutions," *Reg Anesth Pain Med*, vol. 33, no. 6, pp. 532–544, 2008.

[2] T. H. Helbich, W. Matzek, and M. H. Fuchsjäger, "Stereotactic and ultrasound-guided breast biopsy," *Eur Radiol*, vol. 14, no. 3, pp. 383–393, 2004.

[3] F. Daffos, M. Capella-Pavlovsky, and F. Forestier, "Fetal blood sampling during pregnancy with use of a needle guided by ultrasound: A study of 606 consecutive cases," *Am J Obstet Gynecol*, vol. 153, no. 6, pp. 655–660, 1985.

[4] J. P. Rathmell, H. T. Benzon, P. Dreyfuss, M. Huntoon, M. Wallace, R. Baker, K. D. Riew, R. W. Rosenquist, C. Aprill, N. S. Rost, A. Buvanendran, D. S. Kreiner, N. Bogduk, D. R. Fourney, E. Fraifeld, S. Horn, J. Stone, K. Vorenkamp, G. Lawler, J. Summers, D. Kloth, D. O'Brien, and S. Tutton, "Safeguards to prevent neurologic complications after epidural steroid injections: Consensus opinions from a multidisciplinary working group and national organizations," *Anesthesiology*, vol. 122, no. 5, pp. 974–984, 2015.

[5] P. Beard, "Biomedical photoacoustic imaging," *Interface Focus*, vol. 1, no. 4, pp. 602–631, 2011.

[6] M. Kuniyil Ajith Singh, W. Steenbergen, and S. Manohar, "Handheld Probe-Based Dual Mode Ultrasound/Photoacoustics for Biomedical Imaging," in *Frontiers in Biophotonics for Translational Medicine: In the Celebration of Year of Light (2015)*, ser. Progress in Optical Science and Photonics, M. Olivo and U. S. Dinish, Eds. Singapore: Springer, 2016, pp. 209–247.

[7] S. Park, J. Jang, J. Kim, Y. S. Kim, and C. Kim, "Real-time Triple-modal Photoacoustic, Ultrasound, and Magnetic Resonance Fusion Imaging of Humans," *IEEE Transactions on Medical Imaging*, vol. 36, no. 9, pp. 1912–1921, 2017.

[8] W. Xia, M. Kuniyil Ajith Singh, E. Maneas, N. Sato, Y. Shigeta, T. Agano, S. Ourselin, S. J. West, and A. E. Desjardins, "Handheld Real-Time LED-Based Photoacoustic and Ultrasound Imaging System for Accurate Visualization of Clinical Metal Needles and Superficial Vasculature to Guide Minimally Invasive Procedures," *Sensors*, vol. 18, no. 5, p. 1394, 2018.

[9] M. Kuniyil Ajith Singh and W. Xia, "Portable and Affordable Light Source-Based Photoacoustic Tomography," *Sensors*, vol. 20, no. 21, p. 6173, 2020.

[10] M. Kuniyil Ajith Singh, K. Sivasubramanian, N. Sato, F. Ichihashi, Y. Sankai, and L. Xing, "Deep learning-enhanced LED-based photoacoustic imaging," in *Photons Plus Ultrasound: Imaging and Sensing 2020*, A. A. Oraevsky and L. V. Wang, Eds. San Francisco, United States: SPIE, 2020, p. 116.

[11] A. Hariri, A. Hariri, K. Alipour, K. Alipour, Y. Mantri, J. P. Schulze, J. P. Schulze, J. V. Jokerst, J. V. Jokerst, and J. V. Jokerst, "Deep learning improves contrast in low-fluence photoacoustic imaging," *Biomed. Opt. Express, BOE*, vol. 11, no. 6, pp. 3360–3373, 2020.

[12] F. Kalloor Joseph, A. Arora, P. Kancharla, M. Kuniyil Ajith Singh, W. Steenbergen, and S. S. Channappayya, "Generative adversarial network-based photoacoustic image reconstruction from bandlimited and limited-view data," in *Photons Plus Ultrasound: Imaging and Sensing 2021*, A. A. Oraevsky and L. V. Wang, Eds. Online Only, United States: SPIE, 2021, p. 54.

[13] E. M. A. Anas, H. K. Zhang, J. Kang, and E. Boctor, "Enabling fast and high quality LED photoacoustic imaging: A recurrent neural networks based approach," *Biomed. Opt. Express*, vol. 9, no. 8, p. 3852, 2018.

[14] M. A. L. Bell, "Deep learning the sound of light to guide surgeries," in *Advanced Biomedical and Clinical Diagnostic and Surgical Guidance Systems XVII*, vol. 10868. International Society for Optics and Photonics, 2019, p. 108680G.

[15] L. Wang, S. L. Jacques, and L. Zheng, "MCML—Monte Carlo modeling of light transport in multi-layered tissues," *Computer Methods and Programs in Biomedicine*, vol. 47, no. 2, pp. 131–146, 1995.

[16] Q. Fang and D. A. Boas, "Monte Carlo Simulation of Photon Migration in 3D Turbid Media Accelerated by Graphics Processing Units," *Opt. Express, OE*, vol. 17, no. 22, pp. 20 178–20 190, 2009.

[17] B. E. Treeby and B. T. Cox, "K-Wave: MATLAB toolbox for the simulation and reconstruction of photoacoustic wave fields," *JBO*, vol. 15, no. 2, p. 021314, 2010.

[18] S. L. Jacques, "Optical properties of biological tissues: A review," *Phys. Med. Biol.*, vol. 58, no. 11, pp. R37–R61, 2013.

[19] M. Jaeger, S. Schüpbach, A. Gertsch, M. Kitz, and M. Frenz, "Fourier reconstruction in optoacoustic imaging using truncated regularized inverse k -space interpolation," *Inverse Problems*, vol. 23, no. 6, pp. S51–S63, 2007.

[20] A. Hauptmann and B. Cox, "Deep learning in photoacoustic tomography: Current approaches and future directions," *J. Biomed. Opt.*, vol. 25, no. 11, 2020.

[21] H. J. van Staveren, C. J. M. Moes, J. van Marie, S. A. Prahl, and M. J. C. van Gemert, "Light scattering in lntralipid-10% in the wavelength range of 400–1100 nm," *Appl. Opt., AO*, vol. 30, no. 31, pp. 4507–4514, 1991.

[22] W. Xia, S. Noimark, S. Ourselin, S. J. West, M. C. Finlay, A. L. David, and A. E. Desjardins, "Ultrasonic Needle Tracking with a Fibre-Optic Ultrasound Transmitter for Guidance of Minimally Invasive Fetal Surgery," in *Medical Image Computing and Computer-Assisted Intervention - MICCAI 2017*, M. Descoteaux, L. Maier-Hein, P. Jannin, D. L. Collins, and S. Duchesne, Eds. Cham: Springer International Publishing, 2017, vol. 10434, pp. 637–645.

[23] W. Xia, S. Noimark, E. Maneas, N. M. Brown, M. K. A. Singh, S. Ourselin, S. J. West, and A. E. Desjardins, "Enhancing photoacoustic visualization of medical devices with elastomeric nanocomposite coatings," in *Photons Plus Ultrasound: Imaging and Sensing 2019*, vol. 10878. International Society for Optics and Photonics, 2019, p. 108783G.